Shahrood University of Technology

Journal_of Mining and Environment (JME)

Journal homepage: www.jme.shahroodut.ac.ir

Iranian Society of Mining Engineering (IRSME)

Satellite Image Processing: Application for Alteration Separation based on U-Statistic Method in Zafarghand Porphyry System (Iran)

Seyyed Saeed Ghannadpour[1*], Morteza Hasiri[1], Hadi Jalili[2], and Somayeh Talebiesfandarani[2]

1. Department of Mining Engineering, Amirkabir University of Technology, Tehran, Iran
2. Ph.D, Iranian Space Research Center, Tehran, Iran

Article Info	Abstract
	The Zafarghand area (as a porphyry Cu deposit) is located in the northeast of Isfahan and southeast of Ardestan, which is a part of the Iran-Central structural zone, and more precisely, it is located in the Urmia-Dokhtar volcanic belt. In the porphyry Cu deposits exploration, identifying and determining the alteration zones is of special importance. The aim of the present study is to identify and highlight the alteration zones of Zafarghand area, with the help of the U-statistic method in the processing of ASTER sensor satellite images. Accordingly, considering the raster nature and digital form of satellite images, the digital number values of each pixel from the image matrices were considered as samples in a systematic network. Finally, the U spatial statistic algorithm was implemented as a moving window algorithm for determining anomaly samples in the set of digital number (DN) values of ASTER satellite image pixels. The results of this technique show that the application of the U-statistic method, considering its structural nature and neighboring samples in decision-making, has been successful and has proven to be very effective in determining the alteration zones in the Zafarghand area.

1. Introduction

The Tethyan metallogenic belt stretches from Eastern Europe (Romania, Slovakia, and Turkey) to the Middle East (Iran, Pakistan, and Afghanistan). Iran is located on this belt for over 1700 kilometers, and has significant reserves of porphyry copper deposits such as the Sar Cheshmeh deposit. A part of this belt is the Urmia-Dokhtar Magmatic Arc (UDMA). The Zafarghand exploration area (in northeastern Isfahan) is located in the central part of this arc (Figure 1) [1]. In the recent years, numerous studies have been carried out in this area, which will be briefly described below.

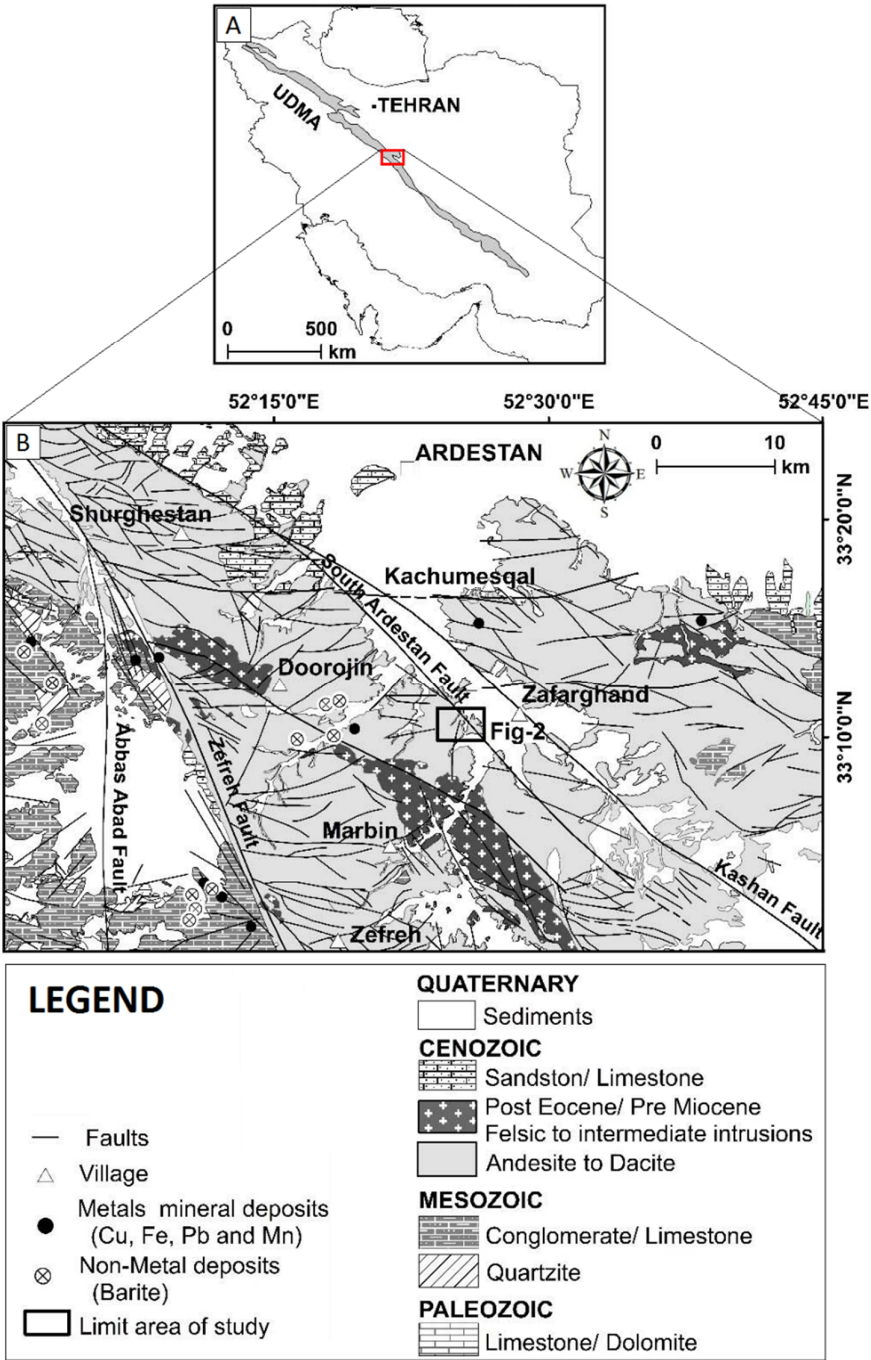✉ Corresponding author: s.ghannadpour@aut.ac.ir (S.S. Ghannadpour)

Figure 1. A: Display of the Zafarghand exploration area in the central section of the UDMA, and B: Part of the simplified Ardestan and Shahrab geological map with a scale of 1:100,000 (after slight modifications from [1-3]) (the location of Figure 2 is also depicted in this figure).

The initial exploration activity in the region involved the preparation of a geological map with a scale of 1:5000, lithological sampling, and preparing geo-physical sections in the area [4].

Subsequent geo-chemical and petrological studies have been conducted on volcanic and volcaniclastic rocks, as well as on neighboring or similar granitoid masses and andesite-basaltic dykes that cut across the Eocene volcanic rocks. These studies were carried out by [5-8]. In 2011, the petrogenesis of the Zafarghand granitoid mass was studied by Sadeghian and Ghafari [5].

Aminoroaya Yamini *et al*. studied the thermal alterations of this deposit with a focus on mineralogical and geo-chemical changes in 2016 [9]. Alaminia *et al*. also examined the geo-

667

chemistry, geo-physics, and fluids inclusions in this area in 2017 [1]. Aminoroaya Yamini *et al*. also investigated the evolution of the magmatic system of this deposit, considering plagioclase as an indicator [10].

In another study, the relationship between mineralization and alteration zones with tectonic structures was investigated by Mohammadi *et al*. with the help of remote sensing studies [11].

In 2016, the chloritization of biotite was analyzed to study the mineralization parameters and associated alteration in the Zafarghand porphyry copper system, using mineral chemistry and stable isotope analysis [12]. Aminoroaya Yamini *et al*. also studied the petrography, geo-chemistry, and alteration thermometry of syno-sedimentary copper mineralization in this area [13]. The isotopic and geochemical constraints on the role of crust-magma mixing in the UMDA were determined, with a focus on the microgranular mafic enclaves and genetic granitoids in the igneous Zafarghand complex [14]. In 2017, the Zafarghand exploration area was considered as a case study for identifying deep and blind mineral deposits using the newly proposed frequency coefficient method in the field of geo-chemical data [15].

Given the importance of this deposit and the need for further comprehensive studies, this research work focuses on processing satellite images from the ASTER sensor in order to identify surface geo-chemical anomalies in this area. Therefore, the U-statistics method is utilized for satellite image processing, which is recognized as an effective method in separating geo-chemical anomalies from the background with a structural nature (i.e. considering the surrounding sample locations in decision-making).

2. Geological setting of Zafarghand porphyry copper system

The Zafarghand copper exploration area is located in southeastern Ardestan, in central Iran, about 110 kilometers northeast of Isfahan. The deposit is situated in the west of Zafarghand, as part of the 1:100,000 Ardestan geological sheet, ranging from $55^{\circ}23'52''E$ to $30^{\circ}26'52''E$ longitude and $52^{\circ}11'33''N$ to $30^{\circ}10'33''N$ latitude (Figure 2) [1]. To access the area, one can use the Ardestan-Naeen road in the western part, Ardestan-Isfahan road in the central section, Zafarghand-Zefreh road in the southern part, and Ardestan-Natanz road in the northern part of the region. The studied deposit is located at the western margin of the Central Iran structural zone and on the central part of the UMDA, similar to other porphyry copper deposits in Iran and worldwide, it had a magmatic origin.
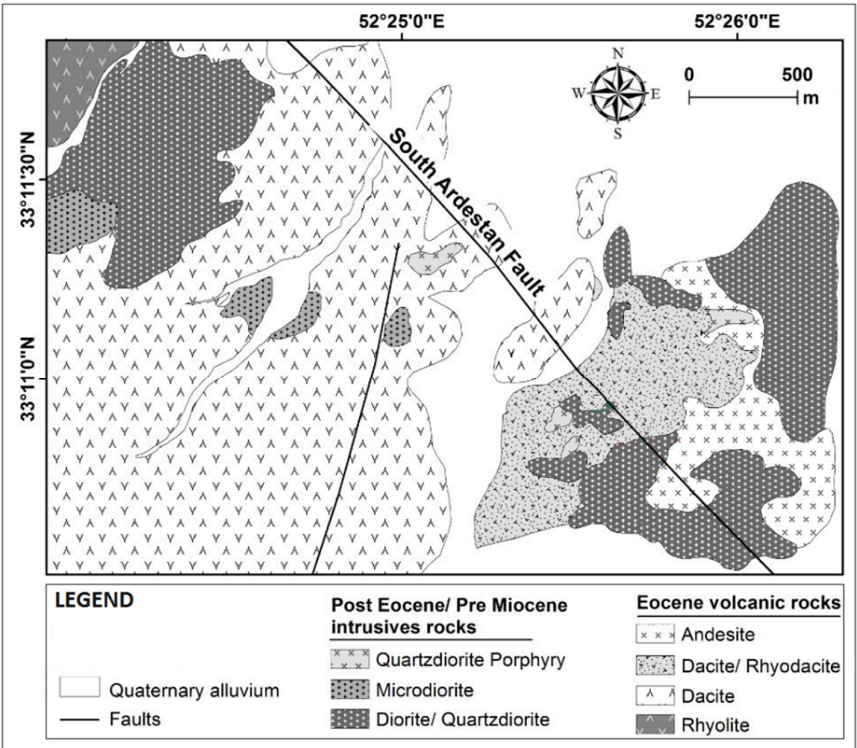

Figure 2. Simplified geological map of the Zafarghand exploration area (modified after [1]).

Based on field investigations and petrography carried out in this area, acidic to intermediate igneous rocks including volcanic and intrusive rocks belonging to the upper Eocene and younger time period are outcrops, which are described in the following rock units [1]. Rhyolite has a relatively small outcrop in the northwest corner with a pinkish gray color (Figure 2). The texture of these rocks is porphyritic with a glassy flow. Dacites and rhyodacites cover a wide range of the area and have gray to greenish colors (Figure 2). This unit is considered the most important host rock for copper mineralization in the region, and has a porphyry texture with fine-grained, amorphous, and porous felsic paste. Andesites are relatively large in the southwestern and western parts of the region (Figure 2), and they appear dark gray and they are hollow due to the abundance of coarse crystals. Intrusive masses of diorite, quartz diorite, and micro-diorite protrude in the northwestern and southeastern parts of the region with a dark gray color (Figure 2). A semi-intrusive porphyritic

quartz diorite mass covers a small area in the southeastern part of the region (Figure 2) [1].

3. Alteration and mineralization

Based on the conducted studies and investigations, the different alterations in the region include potassic, phyllic, siliceous, argillic, and propylitic alterations. These alterations are often observed near intrusive masses and host rocks around the South Ardestan fault (Figure 3) [1]. In the southeastern corner of the area, potassic alteration is very limited near the quartz diorite mass, while phyllic alteration is observed near the intrusive diorite and porphyritic quartz diorite masses, as well as the dacite and rhyodacite volcanic rocks. Siliceous and argillic alterations have limited replacement of phyllic alteration (Figure 3). Propylitic alteration is widespread in the outer area of the deposit (Figure 3) [1]. It should be noted that chlorite is observed in a wide area of the south Ardestan region.
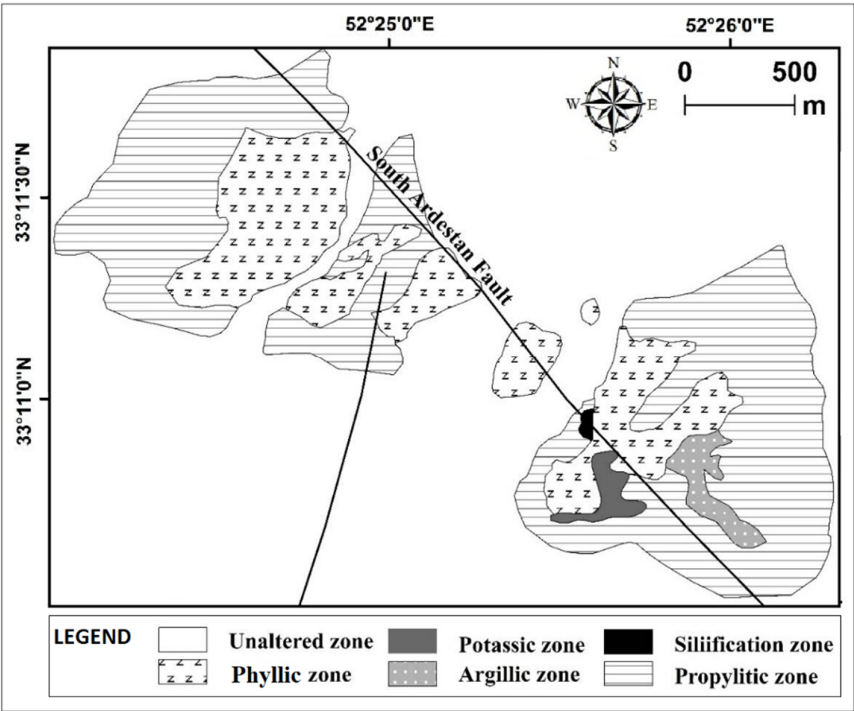

Figure 3. Expansion of halo effects in the Zafarghand exploration area (modified after [1]).

4. Materials and Method
4.1. Data

In line with the main objective of this study and for highlighting various geological anomalies and important indicator minerals in the assessment of mineral potential in the studied area, ASTER satellite images will be utilized.

The ASTER (Advanced Spaceborne Thermal Emission and Reflection Radiometer) sensor is mounted on the Terra satellite, and was launched into space in 1999. The data from this sensor consists of 14 bands as shown in Table 1 [16], with three bands in the VNIR range (0.86-0.52 micrometers) with a spatial resolution of 15 meters, six bands in the SWIR range (2.56-1.6

micrometers) with a spatial resolution of 30 meters, and five bands in the TIR range (11.65-8.25 micrometers) with a spatial resolution of 90 meters. The radiometric resolution is 8 bits for VNIR and SWIR bands, and 12 bits for TIR bands. Each ASTER image covers an area of 60×60 square kilometers. Due to the multiple bands in the SWIR and TIR range, ASTER images have extensive applications in geological studies, particularly in the identification of alteration zones. The SWIR bands of these images cover the absorption ranges of Al-O-H, Si-O-H, and Mg-O-H and could be effective in their identification [17]. Among the reflected infrared bands, 6 bands are designed in the wavelength range of 1.3 to 3.1 micrometers, which are very useful for geological applications (especially mineralogy). The 5 thermal infrared bands are also used for accurate estimation of surface temperature and measurement of various phenomena. In terms of radiometric, the reflected visible and infrared images are designed as 8-bit and the thermal infrared images are designed as 12-bit, which allows for increased radiometric accuracy of the thermal bands [18]. ASTER sensor data are used to identify alteration zones, minerals, and lithology in geological studies. ASTER data, either alone or in combination with other remote sensing satellites and ground data, are used to produce geological maps [19]. ASTER has the capability of being combined with other remote sensing satellites as well. By combining ASTER data with other satellites and sensors, maps with higher accuracy could be generated. In many recent studies, the emphasis has been on the combined use of ASTER data and other remote sensing satellites. The most prominent example of this combination could be seen in Landsat and ASTER data.

The images employed in this study are L1T images for the year 2002, which were chosen because starting from 2008, the 6-band shortwave infrared (SWIR) detector of the ASTER sensor has been completely out of use and its data since then is provided without these mentioned bands on the sites. The use of the 4-band VNIR range of the Landsat sensor is suitable for intermediate metal, especially iron, rare earth elements, and chlorophyll absorption in plants. While the 5-band coverage of the ASTER sensor compared to the 2-band wide Landsat range in the SWIR range has made it possible to distinguish hydroxyl group minerals, hydrates, carbonates, and most importantly, indicative minerals of feldspar, argillaceous, propylitic zones from each other.

Table 1. General specifications of the ASTER sensor [16].

Sub-system	Band No.	Spectral range (m)	Spatial resolutions (m)	Quantization levels
VNIR	1	0.52-0.60	15	8 bits
	2	0.63-0.69		
	3 (N & B)	0.78-0.86		
SWIR	4	1.60-1.70	30	8 bits
	5	2.145-2.185		
	6	2.185-2.225		
	7	2.235-2.285		
	8	2.295-2.365		
	9	2.360-2.430		
TIR	10	8.125-8.475	90	12 bits
	11	8.475-8.825		
	12	8.925-9.275		
	13	10.25-10.95		
	14	10.95-11.65		

4.2. U-statistic

The U-spatial statistic method is considered an effective and powerful method in the field of separation of geochemical anomalies. In fact, the basis of this method is a type of moving average, with the feature that the size of the window in which the averaging takes place changes at each specific point. Therefore, for each specific point, different values are calculated to determine the value of U, based on the surrounding points. In this way, at first, a distance criterion is determined in order to determine the distance and proximity of the sample. Then a specific weight is assigned to each sample based on this measure, and the weighted average value of the points within the search range is calculated to determine their spread for each sample. Finally, the value of U is calculated using the following formula [20-24]:

$$U_i(r) = \frac{\bar{x}_i(r) - \mu}{\sigma}$$

in which μ is the average, r is the neighborhood radius, $x_i(r)$ is the weighted average value of the i-th sample, and σ is the standard deviation of the entire data. The value of $U_i(r)$ is a function of r, meaning that different values for U_i are obtained by changing r. For each r, a number of surrounding samples participate in calculating the value of U for the unknown point. As a result, different U values are obtained for the unknown point, and the highest value (regardless of its sign) is assigned to the sample (considering its sign). One of the advantages of the U-statistic method is its ability to be combined with other methods because this method assigns a new value to the samples. By using this new value (calculated U values), it could be combined with other methods to increase the efficiency of separation [25-27].

Continuing in the results and discussion section, after performing the necessary pre-processing on the satellite images of the ASTER and data preparation, the U spatial statistic algorithm will be applied to the brightness values of each pixel, considering their coordinates. Finally, for enhancing the desired features, the color composite method will be employed. Figure 4. illustrates the steps of this study in the form of a flowchart.

5. Results and Discussion
5.1. Pre-processing of satellite images

In this section, before applying the anomaly structural separation method, the preparation and pre-processing of satellite images will be discussed, because in order to obtain information from satellite images, radiometric and geometric pre-processing is necessary before using them. Pre-processing includes operations that need to be done before the main data analysis and information extraction. Geometric and radiometric corrections are among these operations. Geometric corrections are performed to georeference the image, and radiometric corrections include actions to remove effects such as sunlight passing through clouds, suspended particles in space, oxygen, nitrogen, and other elements that create noise. In other words, radiometric corrections remove the factors that have affected the received spectra and create contrast in the received images.

In this study, geometric correction has already been performed on the desired data, and this data has been georeferenced [28-30], and only radiometric correction needs to be done on these data [28-30]. To eliminate the effects related to

solar radiation, atmospheric transmission, and device errors, the residual logarithmic (Log Residual) method has been used to consider the topographic effects in ASTER images [31]. Moreover, the Internal Average Relative Reflectance (IARR) method is suitable for dry and semi-arid areas due to their sparse vegetation cover and low water vapor and suitable atmospheric conditions. It is also effective for areas where no specific ground measurements are available [31]. The QUick Atmospheric Correction (QUAC) method has been employed to eliminate the effects of absorption and scattering of electromagnetic waves. This method is an atmospheric correction method for the visible, near-infrared, and mid-infrared ranges. This method is applicable for correcting multi-spectral and hyperspectral images in the range of 400 to 3000 nanometers. This algorithm is suitable for correcting images that have been previously prepared or images that do not have atmospheric and ground samples for absolute method application [32].

5.2. Preparing satellite images for data extraction

After applying the aforementioned methods for image preprocessing of the Zafarghand region, in order to prepare the desired image for applying the U-statistic algorithm, the selected region of interest image was resized and bands 4 to 9 of the SWIR range were selected to extract the digital number (DN) values for each selected pixel. The selection of these bands was based on studies conducted on porphyry copper deposits with ASTER data for their employing in band ratio and color composite technique. These bands are considered the most important satellite image bands for enhancing the anomalies of porphyry copper deposits due to their absorption and reflectance characteristics. The resized output of bands 4 to 9 of the SWIR could be seen in Figure 5. as an example. As observed, the quality of the desired image is not very high, which is due to the small size of the studied area compared to a scene of ASTER satellite images and the consequent decrease in the number of pixels. However, this issue not only did not create a problem during the course of this research work, but the visibility of pixels in this image also indicates a distinct sample with known coordinates for applying the U-statistic method and displaying the impact of these methods on the data (DN values of each pixel).
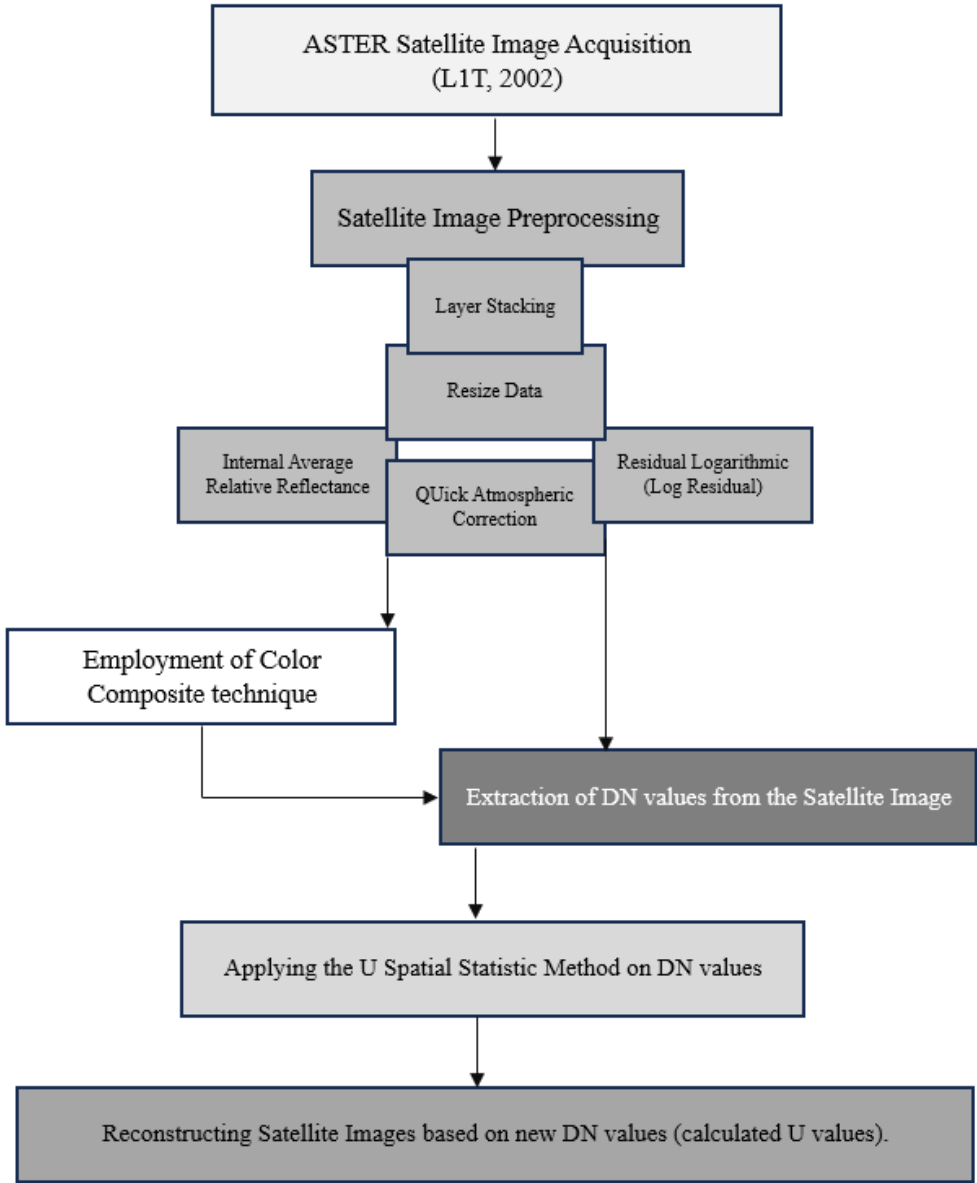
```
              ┌─────────────────────────────────────┐
              │   ASTER Satellite Image Acquisition  │
              │            (L1T, 2002)               │
              └─────────────────────────────────────┘
                                │
                                ▼
              ┌─────────────────────────────────────┐
              │      Satellite Image Preprocessing   │
              └─────────────────────────────────────┘

                       ┌──────────────────┐
                       │  Layer Stacking   │
                       └──────────────────┘

                       ┌──────────────────┐
                       │   Resize Data     │
                       └──────────────────┘

   ┌────────────────────┐  ┌──────────────┐  ┌────────────────────┐
   │ Internal Average   │  │              │  │ Residual Logarithmic│
   │ Relative Reflectance│ │QUick Atmospheric│ │  (Log Residual)    │
   │                    │  │  Correction   │  │                    │
   └────────────────────┘  └──────────────┘  └────────────────────┘

   ┌────────────────────┐
   │ Employment of Color│
   │ Composite technique│
   └────────────────────┘
                      │                              │
                      └──────────┐    ┌──────────────┘
                                 ▼    ▼
              ┌─────────────────────────────────────┐
              │ Extraction of DN values from the Satellite Image │
              └─────────────────────────────────────┘
                                │
                                ▼
              ┌─────────────────────────────────────┐
              │ Applying the U Spatial Statistic Method on DN values │
              └─────────────────────────────────────┘
                                │
                                ▼
   ┌──────────────────────────────────────────────────────────┐
   │ Reconstructing Satellite Images based on new DN values (calculated U values). │
   └──────────────────────────────────────────────────────────┘
```

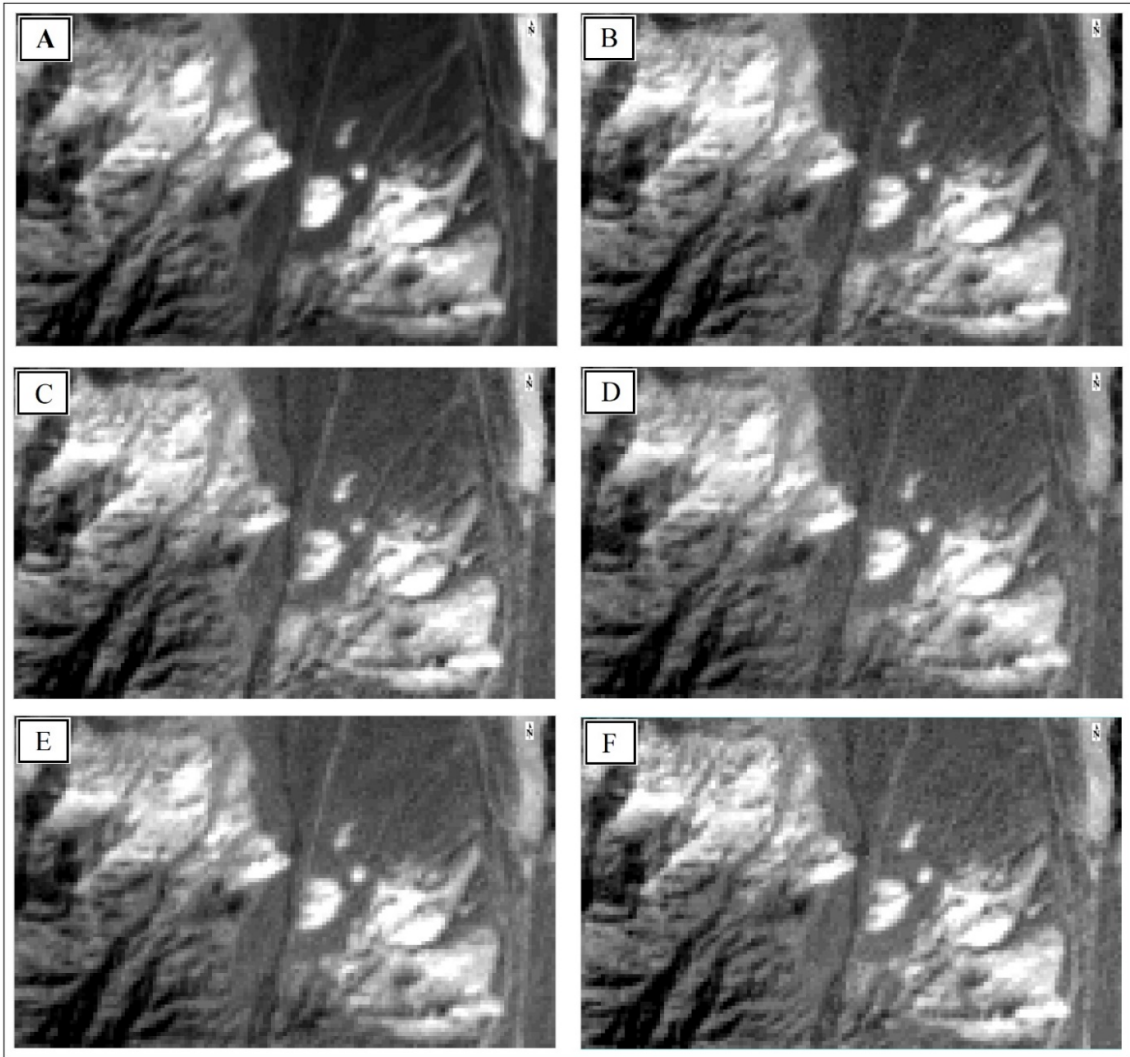**Figure 4. The flowchart of various stages and the process of the task execution.**

Figure 5. Resized ASTER satellite images for the SWIR range in the Zafarghand region. A: Band 4, B: Band 5, C: Band 6, D: Band 7, F: Band 8, and E: Band 9.

The statistical specifications required for implementing the U-statistic method algorithm regarding the DN values for bands 4 to 9 in the SWIR range, and the frequency distribution graph of DN values can be observed in Table 2 and Figure 6, respectively.

Table 2. DN statistical specifications of SWIR range bands (bands 4 to 9).

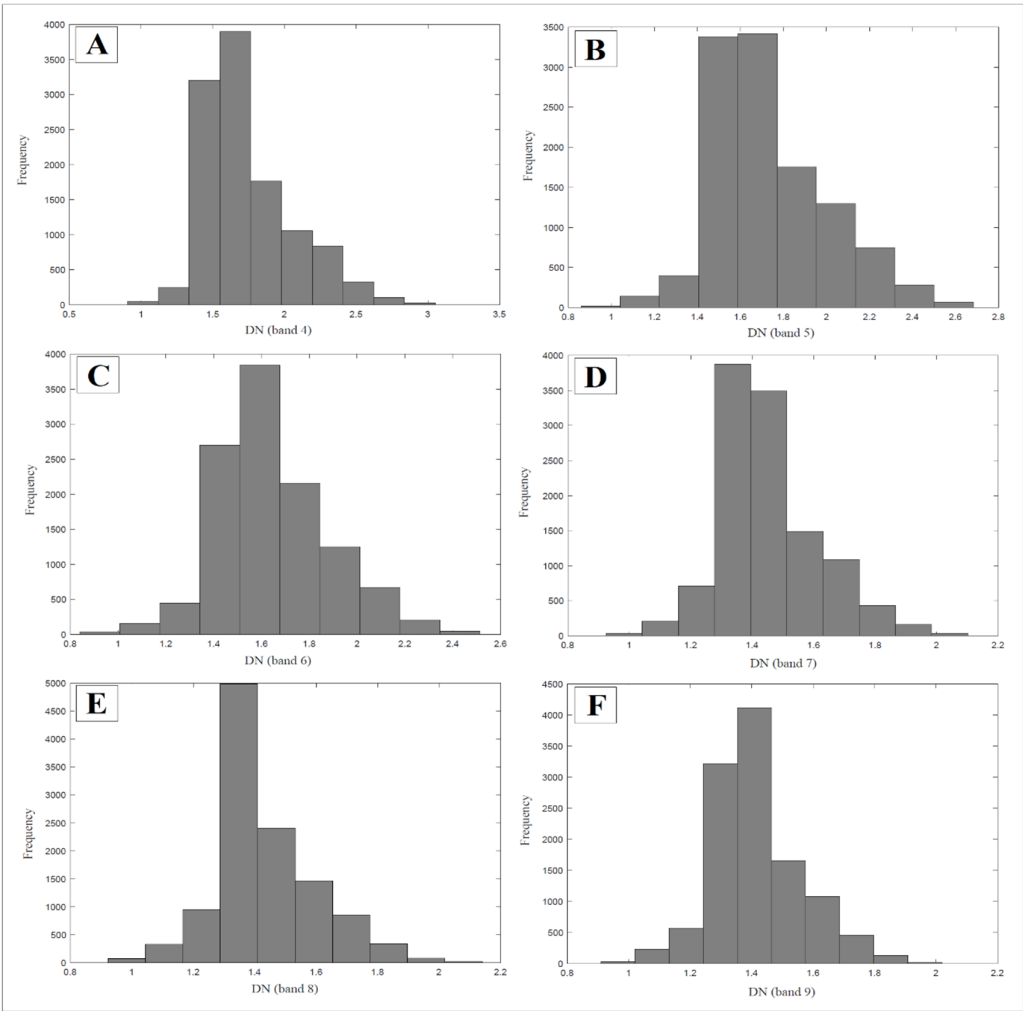| Band	Average	Variance	Standard deviation
4	1.7193	0.0988	0.3143
5	1.7164	0.0708	0.2660
6	1.6378	0.0551	0.2348
7	1.4454	0.0256	0.1601
8	1.4314	0.0279	0.1671
9	1.4126	0.0219	0.1481

Figure 6. Histogram of DN values for the SWIR range. A: Band 4, B: Band 5, C: Band 6, D: Band 7, F: Band 8, and E: Band 9.

As can be seen in Figure 6, the values of DN follow a normal distribution. Therefore, there is no limitation in using the U-statistic method, which conditions normality of the data.

5.3. Applying U-spatial statistics algorithm to DN values

In this section, after extracting the DN values of each pixel from the set of image matrix, the desired values, similar to the samples' concentration related to a systematic dataset (geo-chemical data), along with their initial statistical characteristics and coordinates, are provided as input to the U spatial statistical method. Considering the spatial resolution of 30 meters for the SWIR range, the initial radius value and its incremental value are both set to 18 meters.

After applying the U-statistical algorithm on the DN values of bands 4 to 9 in the SWIR range, the new DN values (i.e. the calculated U values for each pixel based on the DN values of the surrounding pixels) are computed. The statistical characteristics of the calculated U values as the new DN values, and their histogram could be observed in Table 3 and Figure 7, respectively.
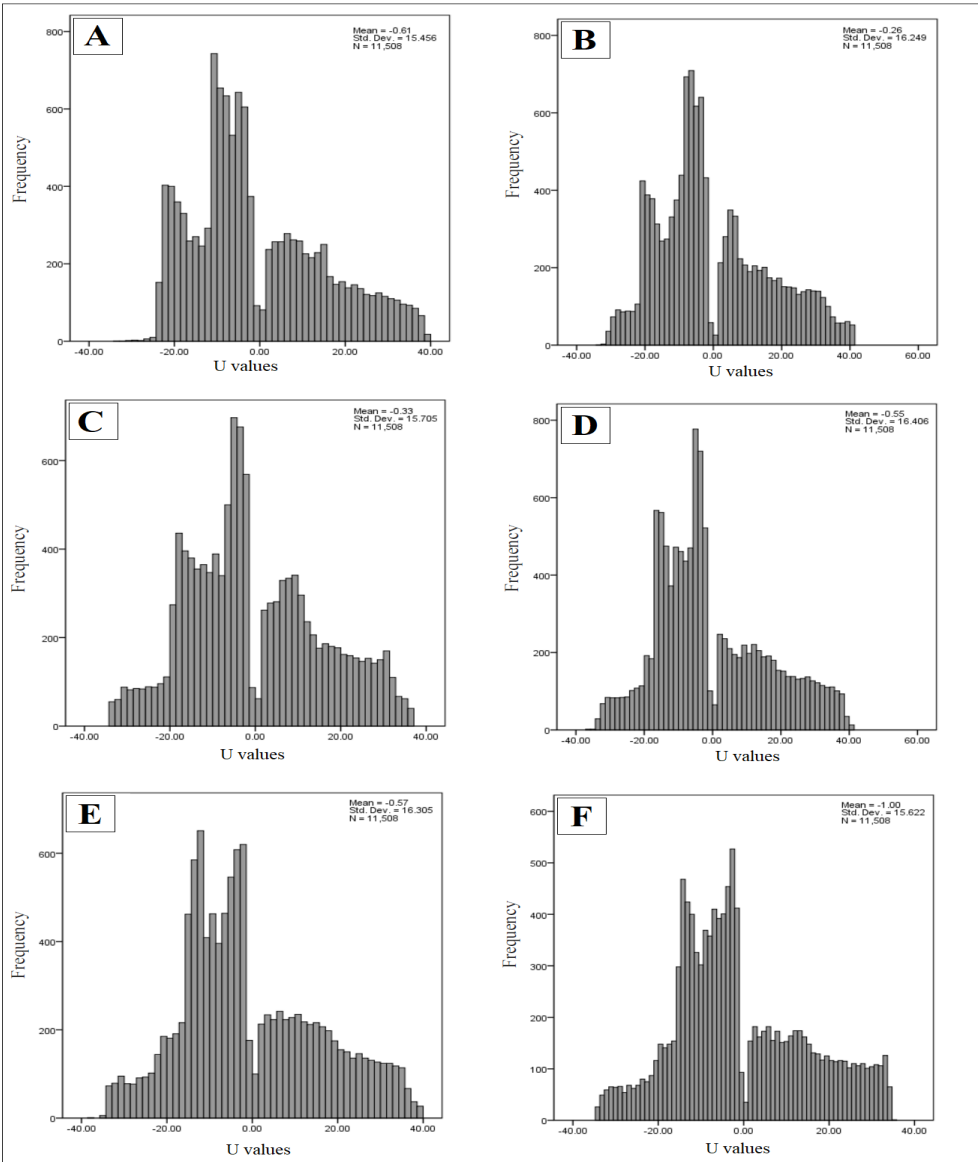
Figure 7. Histogram of the calculated U values for the SWIR range. A: Band 4, B: Band 5, C: Band 6, D: Band 7, F: Band 8, and E: Band 9.

Table 3. U values statistical specifications of SWIR range bands (bands 4 to 9).

Band	Average	Minium	Maximum
4	-0.60512	-33.8226	39.05852
5	-0.25911	-33.5285	41.28934
6	-0.33465	-34.0763	36.55587
7	-0.55412	-36.6264	40.62467
8	-0.57232	-37.1668	39.77979
9	-0.99509	-34.2129	34.74124

As observed in Figure 7, the U values of each pixel or in other words, the new DN values of the image matrix are well-separated from each other at the U = 0 point. In fact, based on this, pixels with higher values are distinguished from those with lower values.

The calculated U values have been replaced as new values of the DN, replacing the previous DN values in the images matrix of SWIR range (bounds 4 to 9), and the obtained results are displayed in Figure 8.
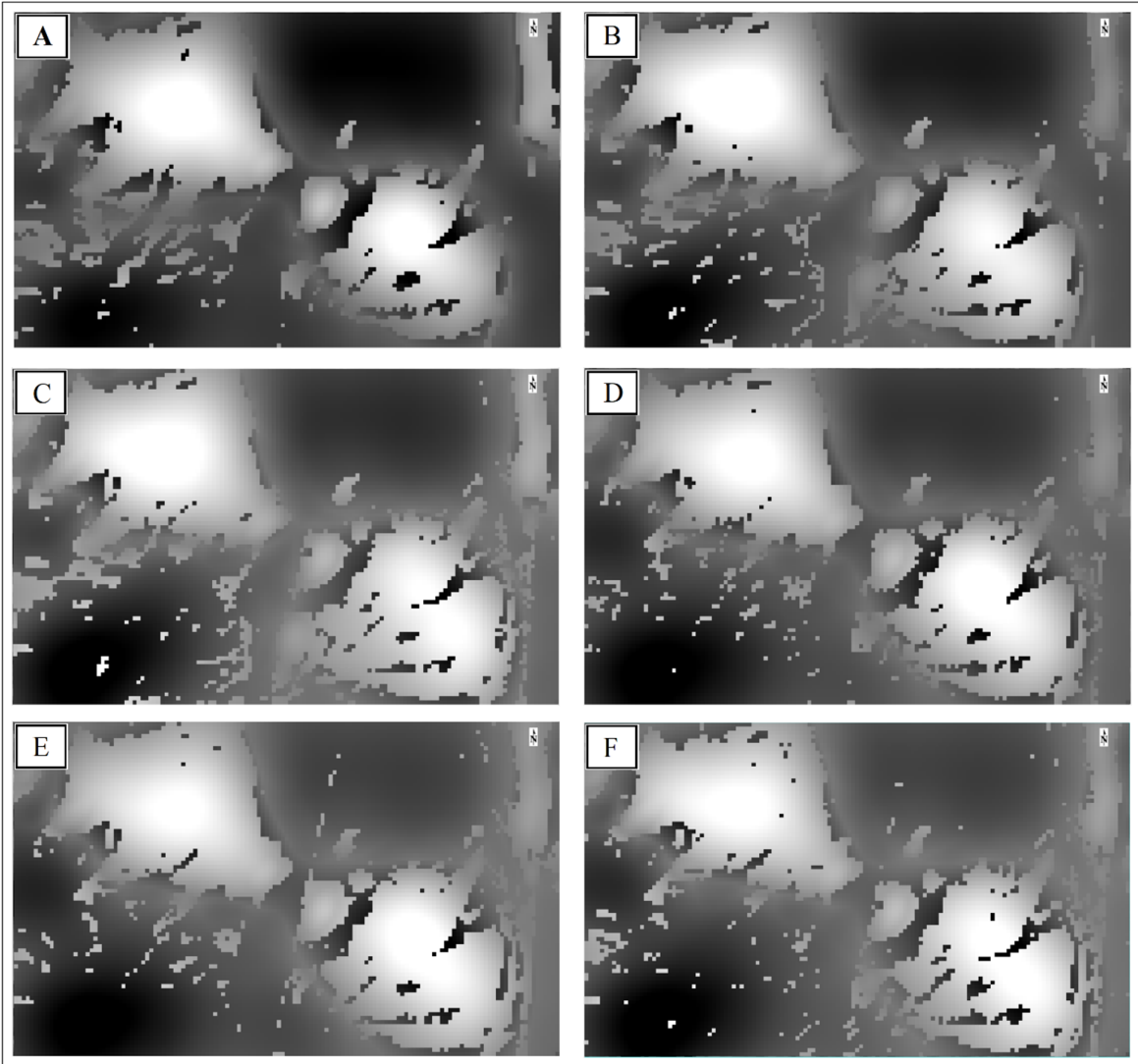
Figure 8. ASTER satellite images with new DN values (calculated U values). A: Band 4, B: Band 5, C: Band 6, D: Band 7, F: Band 8, and E: Band 9.

As can be seen in the above images (Figure 8), the anomalous values are well-separated from the background values, and the desired objective is much clearer in the images than in Figure 5. In this figure, the superiority of images with the U values compared to the initial values of the DN could be observed.

5.4. Enhancement of anomalies using color composite technique

Creating color images is one of the common processing methods in remote sensing investigations. Since satellite images are often available in multi-band formats, examining single-band data at a given time interval does not provide maximum information. Understanding the interrelationships among different wavelengths is crucial for identifying features and various types of land covers. Displaying more than one band simultaneously on an image processing system and creating a multi-band printout can be beneficial and fruitful. This is often achieved through creating color composites and utilizing combined color images. In this case, three bands of data are sent to the red, green, and blue channels of the image display system, resulting in a color image. Simultaneous display of the three image bands in the red, green, blue (R, G, B) channels highlights many phenomena with distinctive colors. In the construction of false color composites, it is preferable to use bands that have less correlation with each other.

The use of colors provides users with more visual and conceptual information from an image. Experimental analyses have shown that an image with the RGB = 468 combination is the most suitable color combination for identifying alteration in most deposits, especially porphyry copper and epithermal gold [30-33]. The false color composite image with ASTER bands 468 is the most comprehensive combination as it clearly differentiates argillic–phyllic alteration (pink) form propylitic alteration (green) [32]. In other word, these RGB (false color composite 468) images typically show argillic and phyllic altered rocks as amethystine tones, and propylitic altered rocks as green tones because of Al-O-H (at ASTER band six) and Fe-, Mg-O-H (at ASTER band eight) absorption features, respectively [33].
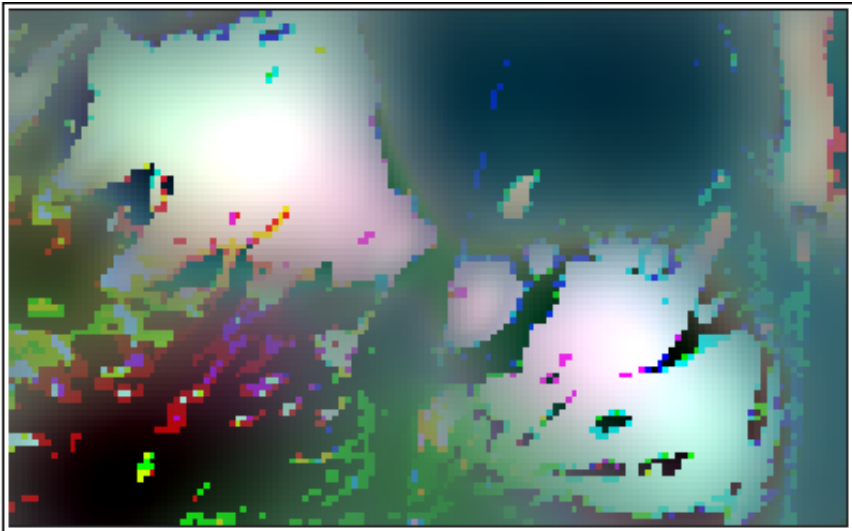

Figure 9. False color composite image with ASTER bands 468 (RGB) based on new DN values (calculated U values).

As seen in the above figure (Figure 9), the propylitic alteration (pale and light green) identified based on the values of U (Figure 10-B) is well-correlated with the propylitic alteration shown in Figure 3. Additionally, the argillic–phyllic alteration (amethystine tones) in Figure 10-A is consistent with the phyllic alteration presented in Figure 3. It is worth mentioning that the identified alterations in the southern region and their inconsistency with the map shown in Figure 3 indicate the lack of geochemical sampling from the southern area. The alteration map depicted in Figure 3 is based on geochemical sampling from the region, and due to the absence of a sampling network design in the Zafarghand exploration zone's southern area, the alterations in the southern region are not represented in this map.
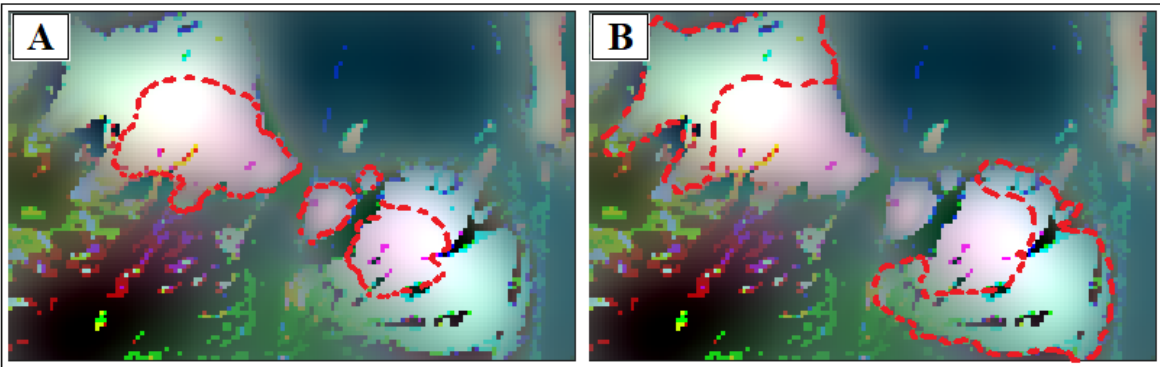

Figure 10. False color composite image with ASTER bands 468 (RGB) based on new DN values. A: Representation of argillic–phyllic alteration, B: Representation of propylitic alteration.

677

The integration of DN values from ASTER images into the Exploration Information System (EIS) represents a significant advancement in the field of mineral prospectivity mapping. As mentioned before, These DN values are indicative of the energy emitted or reflected by the surface, and could be used to identify and characterize various surface features including mineralization related to focused fluid flux. The employing the DN values allows for the creation of weighted alteration layers within the EIS. These layers integrate the spectral information from ASTER, assigning different weights to specific spectral bands based on their relevance to the identification of alteration minerals and mineralization indicators. This approach enables a more targeted and nuanced analysis of the spectral data, enhancing the accuracy of mineral prospectivity mapping. By integrating the weighted alteration layers derived from ASTER DN values into the broader geospatial data framework within the EIS, a comprehensive and multi-dimensional understanding of the mineral potential of a given area is achieved. This integration allows for the combination of spectral information with geological, geochemical, and geophysical data, providing a holistic view of the mineral potential of a specific region. Furthermore, the use of ASTER DN values contributes to the development of prospectivity models within the EIS. These models utilize the weighted alteration layers to prioritize areas with high potential for mineral deposits based on the spectral characteristics captured by ASTER. By incorporating the weighted alteration layers into the prospectivity modeling process, the EIS could generate more accurate and targeted predictions of mineral occurrence [34-40].

Moreover, the relationship between the ASTER DN values and mineralization-related focused fluid flux is crucial for translating this data into mappable exploration targets. Mineralization related to focused fluid flux often exhibits distinct spectral signatures in the shortwave-infrared and thermal infrared regions. Certain minerals associated with hydrothermal alteration and geothermal activity have characteristic absorption features that could be detected in the spectral reflectance captured by ASTER. For example, minerals such as clays, sulfates, carbonates, and hydrothermal alteration products exhibit unique spectral responses in specific wavelength ranges. By analyzing the DN values obtained from ASTER data, particularly in the shortwave-infrared and thermal infrared bands, geoscientists and remote sensing experts can identify and map these mineralogical indicators of focused fluid flux. This integration of remote sensing data with spectral analysis techniques facilitates the translation of mineralization indicators into mappable exploration targets, providing valuable insights for exploration and resource assessment [38, 40-43].

6. Conclusions

In this study, the application of the U-spatial statistic method as a structural approach for separating anomalous values from the background was employed to process satellite images (ASTER sensor imagery) and highlight the alterations of porphyry copper in the Zafarghand exploration zone in the northeast of Isfahan province. Considering the raster and digital nature of satellite images, and consequently, the existence of a regular matrix of DN values for each image, the U statistic encounters a dataset similar to systematic data (similar to geochemical data). Based on the structural nature of the U-statistic method for separating anomalous values, the use of this method was very effective in processing raster-based satellite images. As observed in the results, the newly calculated values for each pixel as U values, through decision-making based on the surrounding DN values, are far more suitable than the initial values of each pixel in the image matrix set. Furthermore, it was observed that the results of contrast enhancement method (false color composite) based on U values in the image matrix set show good conformity with the studied area's alterations. Therefore, the use of processing methods for highlighting and other contrast enhancement methods in remote sensing on the new DN based on the U-statistics method (U-values) seems to be more effective and efficient than their raw values (initial DN), and their employment in other cases is suggested.

References

[1]. Alaminia, A., Bagheri, H., & Salehi, M. (2017). Geochemical and geophysical investigations, and fluid inclusion studies in the exploration area of Zafarghand (Northeast Isfahan, Iran). *Journal of Economic Geology, 9(2)*, 295-312. (In Persian with English Abstract).

[2]. Radfar, J. (1998). Geological map of Ardestan, scale 1:100,000. Geological Survey of Iran, Tehran, Iran.

[3]. Bahroudi, A. (2000). Geological map of Shahrab, scale 1:100,000. Geological Survey of Iran, Tehran, Iran.

[4]. ANJC (Alamut Naghsh-e-Jahan Company), (2011). Initial exploration report of Zafarghand copper index, Isfahan, Iran, 270 p. (in Persian).

[5]. Sadeghian, M. & Ghaffary, M. (2011). The petrogenesis of Zafarghand granitoid pluton (SE of Ardestan). *Petrology, 6*, 47-70. (In Persian with English Abstract).

[6] Amidi, S. M. (1975). Contribution a Í etude stratigraphique, pétrologique et pétrochimique des roches magmatiques de la région Natanz-Nain-Surk (Iran Central). These université scientifique et médicale de Grenoble, France.

[7]. Zahedi, M. & Amidi, S. M. (1975). 1:250000 geological map of Kashan. Geological Survey of Iran, Tehran, Iran.

[8]. Radfar, J., Alaee-Mahabadi, S., & Emami, M.H. (1993). Geological map of Kashan, scale 1:100000. Geological Survey of Iran, Tehran, Iran.

[9]. Aminroayaei Yamini, M., Tutti, F., & Ahmadian, J. (2016). Geochemical and mineralogical evolution of the porphyry copper deposit in southwestern Zafarqand with emphasis on hydrothermal alteration. *Researches in Earth Sciences, 7(1)*, 75-90. (In Persian with English Abstract)

[10]. Aminroayaei Yamini, M., Tutti, F., Aminoroayaei Yamini, M. & Ahmadian, J. (2018). Plagioclase as evidence of magmatic evolution in the Zafarqand porphyry copper deposit, NE Isfahan. *Journal of Economic Geology, 10(1)*, 61-76. (In Persian with English Abstract).

[11]. Mohammadi, S., Nadimi, A., & Alaminia, Z. (2018). Archive of SID Analysis of the relationship between mineralization and alteration zones with tectonic structures using remote sensing studies in south Ardestan area (northeastern Isfahan). *Tectonics, 7*, 29-47. (In Persian with English Abstract).

[12]. Aminoroayaei Yamini, M., Tutti, F., Haschke, M., Ahmadian, j., & Murata, M. (2016). Synorogenic copper mineralization during the Alpine–Himalayan orogeny in the Zafarghand copper exploration district, Central Iran: petrogrography, geochemistry and alteration thermometry. *Geological Journal, 25(2)*, 263-281.

[13]. Aminroayaei Yamini, M., Tutti, F., & Aminoroayaei Yamini, M. (2017). Examination of chloritization of biotite as a tool for reconstructing the physicochemical parameters of mineralization and associated alteration in the Zafarghand porphyry copper system, Ardestan, Central Iran: mineral-chemistry and stable isotope analyses. *Mineralogy and Petrology, 111*, 747-759.

[14]. Sarjoughian, F., Lentz, D., Kananian, A., Ao, S., & Xiao, W. (2018). Geochemical and isotopic constraints on the role of juvenile crust and magma mixing in the UDMA magmatism, Iran: evidence from mafic microgranular enclaves and cogenetic granitoids in the Zafarghand igneous complex. *International Journal of Earth Sciences, 107*, 1127-1151.

[15]. Shahi, H., Ghavami, R., & Kamkar Rouhani, A. (2016). Detection of deep and blind mineral deposits using new proposed frequency coefficients method in frequency domain of geochemical data. *Journal of Geochemical Exploration, 169*, 29-39.

[16]. Biranvandpour, A. & Hashim, M. (2014). ASTER, ALI and Hyperion sensors data for lithological mapping and ore minerals exploration. Springer Plus, 3,130.

[17]. Li, Q., Zhang, B., Lu, L., & Lin, Q. (2014). Hydrothermal alteration mapping using ASTER data in Baogutu porphyry deposit, China, in: IOP Conference Series: Earth and Environmental Science. IOP Publishing, p. 012174.

[18]. Geotz, A., Billingsley, F., Elston, D., Lucchitta, I., Shoemaker, E., Abrams, M., Gillespie, A., & Squries, R. (1975). Applications of ERTS Image and Image Processing to Regional Problems and Geologic Mapping in Northern Arizona. NASA/JPL Technical Reports 32-1597, NASA: Pasadena, CA, USA.

[19]. Plafcan, D. Technoscientific Diplomacy, (2011). The practice of international policies in the ASTER collaboration, In Land Remote Sensing and Global Environmental Change. Ramachandran, R., Justice, C., Abrams, M., Eds., Springer: New York, NY, USA; Chapter 4, pp. 483-508.

[20]. Ghannadpour, S. S. & Hezarkhani, A. (2016). Introducing 3D U-statistic method for separating anomaly from background in exploration geochemical data with associated software development. *Journal of Earth System Science. 125(2)*, 387–401.

[21]. Ghannadpour, S. S., Hezarkhani, A., Maghsoudi, A., & Farahbakhsh, E. (2015). Assessment of prospective areas for providing the geochemical anomaly maps of lead and zinc in Parkam district, Kerman, Iran. *Geosciences Journal, 19(3)*, 431–440.

[22]. Ghannadpour, S. S. & Hezarkhani, A. (2017). Comparing U-statistic and nonstructural methods for separating anomaly and generating geochemical anomaly maps of Cu and Mo in Parkam district, Kerman, Iran. *Carbonates and Evaporites, 32(3)*, 155-166.

[23] Ghannadpour, S. S., Hezarkhani, A., & Sabetmobarhan A. (2017). The Parkam exploration district (Kerman, Iran): Geology, alterations, and delineation of Cu- and Mo-mineralized zones using U-spatial statistic with associated software development. *Journal of Earth Sciences. 28(2)*, 283–294.

[24]. Ghannadpour, S. S., Hezarkhani, A., & Roodpeyma, T. (2017). Combination of Separation Methods and Data Mining Techniques for Prediction of Anomalous Areas in Susanvar, Central Iran. *African Journal of Earth Sciences, 134*, 516–525.

[25]. Ghannadpour, S. S. & Hezarkhani, A. (2018). Providing the bivariate anomaly map of Cu–Mo and Pb–Zn using combination of statistic methods in Parkam

district, Iran. *Carbonates and Evaporites, 33(3)*, 403-420.

[26] Ghannadpour, S. S., Hezarkhani, A., & Sharifzadeh, M. (2017). A method for extracting anomaly map of Au and As using combination of U-statistic and Euclidean distance methods in Susanvar district, Iran. *Journal of Central South University, 24(11)*, 2693–2704.

[27]. Ghannadpour, S. S. & Hezarkhani, A. (2020). Mineral potential mapping for Au and As using Gap statistic method in multivariate mode. *Carbonates and Evaporites, 35(1)*, 1-11.

[28]. Beiranvand Pour, A. & Hashim, M. (2011). Identification of hydrothermal alteration mineral for exploration of porphyry copper deposit using ASTER data, SE Iran. *Journal of Asian Earth Sciences, 42*, 1309-1323.

[29]. Oleson, R. & Doescher, Ch. (2022). Advance Spaceborne Thermal Emission and Reflection Radiometer (ASTER) Level 1 Precision Terrain Corrected Registered At-sensor Radiance Product (AST_L1T). Department of the Interior U.S Geological Survey, 16 p.

[30]. Boloki, M.; Poormirzaee, R. (2009). Using ASTER Image Processing for Hydrothermal Alteration and Key Alteration Minerals Mapping in Siyahrud area, IRAN. *International Journal of Geology, 3*, 38–43.

[31]. Alimohammadi, M., Alirezaei, S., & Kontak, D. J. (2015). Application of ASTER data for exploration of porphyry copper deposits: A case study of Daraloo-Sarmeshk area, southern part of the Kerman copper belt, Iran. *Ore Geology Reviews, 70*, 290–304.

[32]. Testa, F.J., Villanueva, C., Cooke, D.R., & Zhang, L. (2018). Lithological and Hydrothermal Alteration Mapping of Epithermal, Porphyry and Tourmaline Breccia Districts in the Argentine Andes Using ASTER Imagery. *Remote Sensing, 10*, 203.

[33]. Fakhari S, Jafarirad A, Afzal P, & Lotfi M. (2019). Delineation of hydrothermal alteration zones for porphyry systems utilizing ASTER data in Jebal barez area, SE Iran. *Iran Journal of Earth Sciences, 11*, 80–92.

[34]. Sikakwe, G. U. (2023). Mineral exploration employing drones, contemporary geological satellite remote sensing and geographical information system

(GIS) procedures: A review. *Remote Sensing Applications: Society and Environment, 31*.

[35]. Yousefi, M., Carranza, E. J. M., Kreuzer, O. P., Nykänen, V., Hronsky, J. M. A., & Mihalasky, M. J. (2021). Data analysis methods for prospectivity modelling as applied to mineral exploration targeting: State-of-the-art and outlook. *Journal of Geochemical Exploration, 229*, 106839.

[36]. Yousefi, M., Kreuzer, O. P., Nykänen, V., & Hronsky, J. M. A. (2019). Exploration information systems – A proposal for the future use of GIS in mineral exploration targeting. *Ore Geology Reviews, 111*, 103005.

[37]. Yousefi, M. (2017). Recognition of an enhanced multi-element geochemical signature of porphyry copper deposits for vectoring into mineralized zones and delimiting exploration targets in Jiroft area, SE Iran. *Ore Geology Reviews, 83*, 200–214.

[38]. Calvin, W. M., Littlefield, E. F., & Kratt, C. (2015). Remote sensing of geothermal-related minerals for resource exploration in Nevada. *Geothermics, 53*, 517–526.

[39]. Haldar, S. K. (2013). Chapter 6 - Photogeology, Remote Sensing and Geographic Information System in Mineral Exploration. Mineral Exploration, pp. 95–115. Elsevier.

[40]. Knyihár, A., & Winkler, G. (1993). Environmental information system and remote sensing. *Computers, Environment and Urban Systems, 17(3)*, 217-221.

[41]. Yousefi, M. & Hronsky, J. M. A. (2023). Translation of the function of hydrothermal mineralization-related focused fluid flux into a mappable exploration criterion for mineral exploration targeting. *Applied Geochemistry, 149*, 105561.

[42]. Ja'afar Abubakar, A., Hashim, M., Beiranvand Pour, A., & Shehu, K. (2017). A Review of Geothermal Mapping Techniques Using Remotely Sensed Data. *Science World Journal, 12(4)*.

[43]. Achieng, J., Mutua, J., Mibei, G., Olaka, L., & Waswa, A. K. (2017). Mapping of Hydrothermal Minerals Related to Geothermal Activities Using Remote Sensing and GIS: Case Study of Paka Volcano in Kenyan Rift Valley. *International Journal of Geosciences, 8(5)*, 711–725.

پردازش تصویر ماهواره‌ای: جداسازی دگرسانی بر اساس روش آماره فضایی U در سیستم پورفیری ظفرقند

سید سعید قنادپور[1]*، مرتضی حصیری[1]، هادی جلیلی[2]، و سمیه طالبی اسفندارانی[2]

۱. دانشکده مهندسی معدن، دانشگاه صنعتی امیرکبیر (پلی‌تکنیک تهران)، تهران، ایران

۲. مرکز تحقیقات فضایی، پژوهشگاه فضایی ایران، تهران، ایران

چکیده:

منطقه اکتشــافی ظفرقند به عنوان یک کانسار مس پورفیری در شمال شــرق اصفهان و جنوب شــرق اردســتان واقع شــده است که بخشــی از زون ســاختاری ایران مرکزی بوده و به طور دقیق‌تر در کمربند آتشفشانی ارومیه-دختر قرار دارد. در اکتشاف کانسارهای مس پورفیری، شناسایی و تعیین پهنه‌های دگرسانی از اهمیت ویژه‌ای برخوردار است. هدف پژوهش حاضر، شناسایی و تعیین زون‌های دگرسان منطقه ظفرقند با استفاده از روش آماره فضایی U در پردازش تصاویر ماهواره‌ای ســنجنده اســتر است. بر این اساس، با توجه به ماهیت رســتری و شکل رقومی تصاویر ماهواره‌ای، مقادیر دیجیتال نامبر هر پیکسل از مجموعه ماتریس تصاویر، به عنوان یک نمونه در شبکه‌ای سیستماتیک در نظر گرفته شده است. در نهایت نیز روش آماره فضایی U به عنوان یک پنجره متحرک در تعیین نمونه‌های آنومال، بر روی مجموعه مقادیر دیجیتال نامبر پیکسل تصاویر ماهواره‌ای اســتر پیاده شده است. نتایج حاصله از تکنیک فوق‌الذکر نشان می‌دهد بکارگیری روش آماره U با توجه به ماهیت ســاختاری بودن آن و در نظر گرفتن نمونه‌های اطراف در تصــمیم‌گیری، موفقیت آمیز بوده و در تعیین زون‌های دگرســانی منطقه ظفرقند بســیار موثر عمل کرده است.

کلمات کلیدی: آماره U، پردازش تصاویر ماهواره‌ای، استر (ASTER) ، ظفرقند، مس پورفیری.